Plasmonic Optical Nonlinearities of Copper Sulfide Nanoparticles

Plasmonic Optical Nonlinearities of Copper Sulfide Nanoparticles

Yasushi Hamanaka[1], Tatsunori Hirose[1], Kaoru Yamada[1], Kazuki Miyagawa[1], and Toshihiro Kuzuya[2]

[1]*Nagoya Institute of Technology, Gokiso-cho, Showa-ku, Nagoya, Aichi 466-8555, Japan.*

[2]*Muroran Institute of Technology, Mizumoto-cho, Muroran, Hokkaido 050-8585, Japan.*

ABSTRACT

Spherical $Cu_{2-x}S$ nanoparticles with an average diameter of 4.6 nm were synthesized by a colloidal method, and their optical nonlinearities around localized surface plasmon resonance in the near-infrared region were investigated. Resonant enhancement of nonlinear absorption, which is similar to that in the case of the noble metal nanoparticles in the visible region, was observed. The nonlinear absorption coefficients of the $Cu_{2-x}S$ nanoparticles were smaller as compared with those of Au nanoparticles with the same dimensions and concentrations. Theoretical simulation of electric field distributions around individual nanoparticles suggested that the free carrier concentration in $Cu_{2-x}S$ nanoparticles was one order of magnitude smaller than that in Au nanoparticles, which led to a weaker local electric field and weaker optical nonlinearity.

INTRODUCTION

Localized surface plasmon resonance (LSPR) of heavily doped semiconductor nanoparticles (NPs) has attracted significant attention as a strong candidate for plasmonic devices, which are responsible to near-infrared (NIR) light and possess tunable LSPR frequencies due to carrier doping [1-5]. Plasmonic NPs based on noble metals exhibit strong third-order optical nonlinearities owing to local-field enhancement effect by LSPR excitation in the visible frequency region [6]. Therefore, the NIR-LSPR in plasmonic semiconductor NPs makes them potential candidates for application in all-optical switching devices based on the Kerr-type optical nonlinearity corresponding to optical fiber communications. The third-order nonlinear susceptibility $\chi^{(3)}$ of NP dispersions with the volume fraction of NPs being p can be expressed as follows [7]:

$$\chi^{(3)} = p{f_l}^2|f_l|^2{\chi_{NP}}^{(3)}, \qquad (1)$$

where $\chi_{NP}^{(3)}$ is the third-order susceptibility of the NP and f_l is a local-field enhancement factor represented by the following equation:

$$f_l = \frac{E_l}{E_0} = \frac{3\varepsilon_m}{\varepsilon(\omega)+2\varepsilon_m}. \qquad (2)$$

This relation is based on the Maxwell-Garnett theory, where E_0 and E_l are electric fields of the incident light and the local field, respectively; $\varepsilon(\omega)$ and ε_m are the dielectric functions of the NP and the surrounding material, respectively [7]. These theoretical expressions indicate that third-order optical nonlinearities of plasmonic NP dispersions are strongly dependent on the effect of local-field enhancement.

In this study, we investigated the third-order optical nonlinear properties of $Cu_{2-x}S$ NPs, which are some of the best known plasmonic semiconductor NPs. Nonlinear absorption coefficients were measured around the LSPR and compared with those of typical metal NPs, e.g. Au NPs, by simulation of local-field effects.

EXPERIMENTAL

Copper sulfide NPs were synthesized via the solution chemistry route reported by Kuzuya *et al*. [8]. Brief, 0.4 mmol of copper acetate and 8 mmol of octylamine were mixed in toluene and heated up to 363 K under argon gas flow. After heating for 30 min, 0.8 mmol of sulfur powder dissolved in 1-dodecanethiol (10 mmol) was injected quickly. The mixture was stirred for 30 min at 363 K, and then purified by repeated precipitation-redispersion cycles using ethanol and hexane. Finally, copper sulfide NPs dispersed in hexane were obtained.

The sizes and shapes of the NPs were measured by scanning transmission electron microscopy (STEM, JEOL JEM-2100F). The crystalline structure was determined by X-ray diffraction (XRD) analysis of the NPs deposited onto a glass substrate. Elemental composition was investigated by energy-dispersive X-ray spectroscopy (EDX, Horiba EMAX-7000) and X-ray photoelectron spectroscopy (XPS, ULVAC-PHI PHI-5000). The absorption spectrum of copper sulfide NPs dispersed in hexane was obtained by a standard double-beam spectrophotometer (JASCO V-570). Nonlinear absorption coefficients, β, were determined using a pulsed laser system with a pulse duration of 2 ps and repetition rate of 1 kHz (Spectra Physics Millenia-Tsunami, Quantronix Titan, and Quantronix TOPAS). For comparison with standard metallic plasmonic NPs, nonlinear absorption measurements were carried out using an aqueous solution of citrate-stabilized spherical Au NPs with an average diameter of 5 nm (Sigma-Aldrich) around the LSPR peak in the visible region, using the same instruments.

Electric field distribution around the NPs under light illumination was calculated by the finite difference time domain (FDTD) method, using commercial software (Lumerical FDTD solutions).

DISCUSSION

Figure 1 shows the XRD pattern of the NPs. Four diffraction peaks could be assigned to cubic Cu_2S or $Cu_{1.8}S$. The composition ratio between copper and sulfur, Cu/S, was found to be about 1.57 and 1.47, as determined by XPS and EDX, respectively. These

results suggested that Cu-deficient Cu_2S NPs, i.e., $Cu_{2-x}S$ NPs were successfully synthesized; however, it was difficult to estimate the accurate composition because the S atoms could not be distinguished easily in the NP body and in the surfactant, 1-dodecanethiol. The size distribution of the NPs, determined from STEM observations, is shown in the inset of Fig. 1, where the average diameter of the NPs is found to be 4.6 nm.

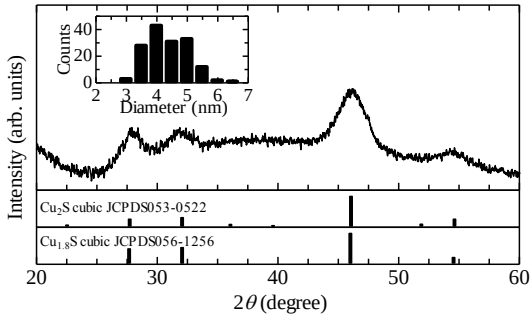

Figure 1. XRD pattern of $Cu_{2-x}S$ NPs, with the standard diffraction data of cubic Cu_2S and $Cu_{1.8}S$. The inset shows the size distribution of NPs determined by STEM.

In the absorption spectrum of $Cu_{2-x}S$ NPs dispersed in hexane (Fig. 2 (a)), a strong LSPR band could be seen clearly in the NIR region. The peak position and FWHM of the LSPR band were 0.98 and 0.66 eV, respectively. The free carrier concentration, N, in an NP was evaluated from these spectral parameters [9]. In this estimation, the effective mass of a hole reported for $Cu_{1.8}S$, i.e., $1.8m_0$ was used, where m_0 is the free electron mass, because the LSPR in $Cu_{2-x}S$ NPs was due to the excess holes created in the top of the valence band [10,11]. N was determined to be 7.6×10^{21} cm^{-3} from this analysis, which indicated the heavily doped character of the $Cu_{2-x}S$ NPs.

Figure 2(b) shows the absorption coefficients of the NP dispersions embedded in a 1 mm quartz cell and measured by incident laser pulses at various intensities and frequencies around the LSPR peak. Absorption saturation behavior could be clearly observed, especially in the higher-intensity region. Such behavior has previously been observed for the LSPR of noble metal NPs and well explained in terms of hot electron creation and modification of the dielectric function of the NPs produced thereby.

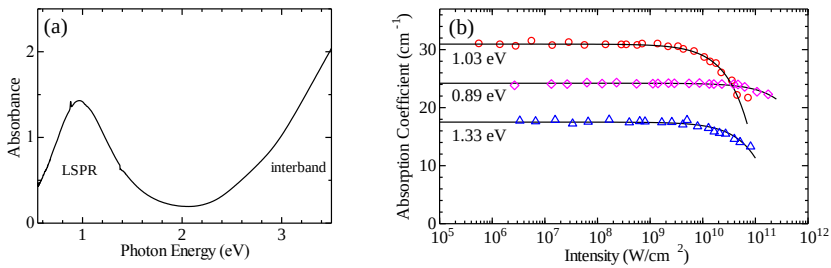

Figure 2. (a) Absorption spectrum of $Cu_{2-x}S$ NPs dispersed in hexane. (b) Absorption saturation behavior of $Cu_{2-x}S$ NPs, measured by incident laser pulses at various frequencies.

The nonlinear absorption coefficients, β, of $Cu_{2-x}S$ NPs were obtained by fitting the absorption curves shown in Fig. 2(b) using the relation $\alpha = \alpha_0 + \beta I$, with β as an adjustable parameter (where α, α_0, and I are an absorption coefficient, linear absorption coefficient, and incident laser intensity) [12]. The obtained values of β are plotted in Fig. 3 in conjunction with a linear absorption spectrum. In the same figure, the β values and absorption spectrum obtained for Au NPs dispersed in water are also shown. The volume fraction of Au NPs was 4×10^{-6} and that of $Cu_{2-x}S$ NPs was to be $\sim4\times10^{-5}$ from the molar absorption coefficient reported for $Cu_{2-x}S$ NPs [1]. The β values of both types of NPs were negative and exhibited resonance behavior similar to the LSPR bands. The largest negative values were -0.197 ± 0.010 and -0.031 ± 0.003 cm/GW for the $Cu_{2-x}S$ and Au NPs, respectively. The estimated value of β of $Cu_{2-x}S$ NPs was one order of magnitude larger than that of the Au NPs. However, it should be taken into account the NP concentration of the $Cu_{2-x}S$ sample was 10 times that of the Au sample; the absorption coefficient of the NP dispersion was proportional to the number concentration of the NPs. Consequently, the β value of the $Cu_{2-x}S$ NPs was two-third that of the Au NPs after converted into the same NP concentrations. This result suggests that the local-field enhancement effect is weaker in $Cu_{2-x}S$ NP compared to that in Au NP, because the nonlinear optical susceptibility of plasmonic NPs is highly sensitive to the local field, as shown in Eq. (2).

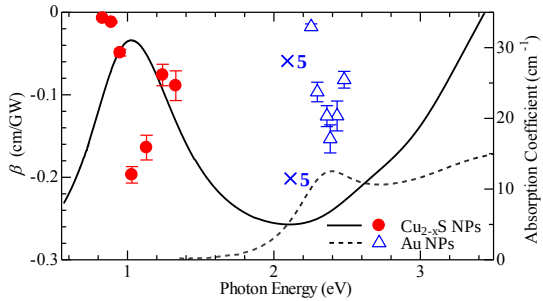

Figure 3. Nonlinear absorption coefficients of $Cu_{2-x}S$ (solid dots) and Au (open dots) NPs. Solid and dotted curves are absorption spectra of the same NPs.

In order to estimate magnitude of the local-field generated around these NPs, electric-field distributions around single $Cu_{2-x}S$ and Au NPs were calculated by the FDTD method. In this calculation, the dielectric function represented by the Drude model with estimated carrier concentration values of 7.6×10^{21} cm^{-3} was used for a $Cu_{2-x}S$ NP, because reliable data for the dielectric function of $Cu_{2-x}S$ are not yet known, especially in the NIR region [13]. The dielectric function of bulk Au was used for the calculation of an Au NP [13]. In the Drude model, the effective mass of the valence band holes of $Cu_{1.8}S$, i.e., $1.8m_0$, was used (where m_0 is the free electron mass) and a damping constant for the carriers was set to reproduce the width of the LSPR band. The refractive index of the surrounding medium was set to 1.33 (water) and 1.37 (hexane) for the Au and $Cu_{2-x}S$ NPs, respectively. Spherical NPs with diameters of 4.6 nm ($Cu_{2-x}S$) and 5 nm (Au) and linearly polarized incident light were assumed. Figure 4(a) shows the simulated spectra of the absorption cross-section. The LSPR absorption bands observed in the NIR and visible regions, as shown in the experimental spectra, could be well reproduced in the simulated spectra.

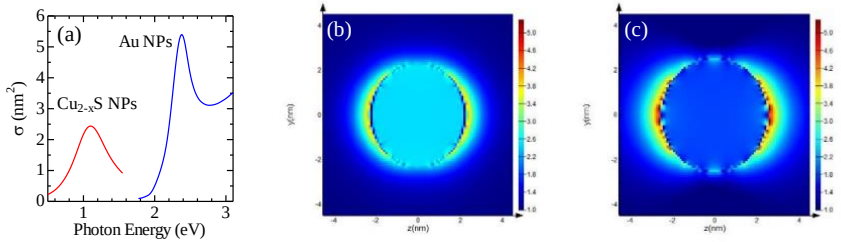

Figure 4. Results of the simulation by the FDTD calculations: (a) Absorption cross-section spectra near the LSPR calculated for a $Cu_{2-x}S$ NP with a diameter of 4.5 nm in hexane (solid curve) and for an Au NP with a diameter of 5 nm in water (dotted curve). Electric field distribution around a single NP of (b) $Cu_{2-x}S$ and of (c) Au upon irradiation by linearly polarized light with the respective resonance frequencies.

Figs. 4(b) and (c) show electric field distributions generated around these NPs under illumination by light with LSPR frequencies. Dipolar-type distribution of the local electric-field was clearly seen in both cases, with hot spots near the NP surfaces. The results indicated that the enhancement factor of the electric field, $|\boldsymbol{E}/\boldsymbol{E}_0|$ ($\boldsymbol{E}_0$ and $\boldsymbol{E}$ are electric field of the incident light and the generated field), reach 4 and 5.3 for the $Cu_{2-x}S$ and Au NPs, respectively. Such a weak field enhancement in the $Cu_{2-x}S$ NP is consistent with our assumption.

The origin of the local electric field is the giant electric polarization formed inside the NP as a result of the resonant excitation of the LSPR. The electric polarization is generated by the collective oscillation of free carriers. Therefore, the free carrier concentration is suggested to be a dominant factor determining the magnitude of the electric polarization, and thus, the local field enhancement. To test this hypothesis, electric field enhancement factors were evaluated for $Cu_{2-x}S$ NPs with various carrier concentrations by the FDTD method. Fig. 5 shows maximum enhancement factors of the electric field, $|\boldsymbol{E}_{max}/\boldsymbol{E}_0|$, evaluated for hole concentrations between 4×10^{21} and 1×10^{22} cm^{-3}. The result of this simulation indicates that the enhancement factor increases monotonically with an increase of carrier concentrations. From this results, we concluded that low electric field enhancement in the $Cu_{2-x}S$ NP is due to the lower free carrier concentration (7.6×10^{21} cm^{-3}) as compared with that for Au (5.9×10^{22} cm^{-3}) [14]. Therefore, the differences in the nonlinear absorption coefficients between the $Cu_{2-x}S$ and Au NPs were ascribed to the same reason.

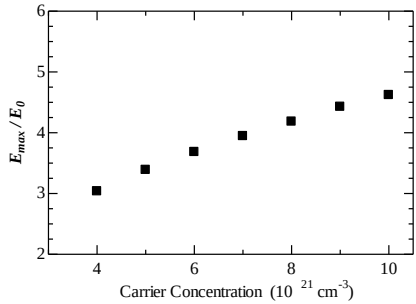

Figure 5. Maximum enhancement factors of the electric field, $|\boldsymbol{E}_{max}/\boldsymbol{E}_0|$, calculated for $Cu_{2-x}S$ NPs at various hole concentrations.

CONCLUSIONS

Spherical $Cu_{2-x}S$ NPs with an average diameter of 4.6 nm and hole concentration of 7.6×10^{21} cm^{-3} were chemically synthesized in solution phase. The $Cu_{2-x}S$ NPs exhibited resonant behavior in nonlinear absorption around the LSPR, similar to the case of the Au NPs. The nonlinear absorption coefficients of the $Cu_{2-x}S$ NPs were 30~40 % smaller than those of the Au NPs with the same dimensions and concentrations. The lower optical nonlinearity in the $Cu_{2-x}S$ NPs could be ascribed to the weaker local electric field, which originated from the lower free carrier concentration in the $Cu_{2-x}S$ NPs with reference to the free electron concentration of metal NPs. However, the $Cu_{2-x}S$ NPs have an outstanding capability as nonlinear optical materials in the NIR region from viewpoints of cost and environment safety, because they consist of only earth-abundant and nontoxic elements. Further progress in carrier doping technique and size- and shape-control methods can promise improvement in optical nonlinearities of the $Cu_{2-x}S$ NPs.

ACKNOWLEDGMENTS

This work was supported by Japan Society of the Promotion of Science (JSPS), KAKENHI Grant Number 26400316, and the grant from the Kurata Memorial Hitachi Science and Technology Foundation. The authors are grateful to Nanotechnology Platform Program (Molecule and Material Synthesis) of the Ministry of Education, Culture, Sports, Science, and Technology (MEXT), Japan.

REFERENCES

1. J.M. Luther, P.K. Jain, T. Ewers, and A.P. Alivisatos, Nature Mater. **10**, 361 (2011).
2. R.J. Mendelsberg, G. Garcia, H. Li, L. Manna, and D.J. Milliron, J. Phys. Chem. C **116**, 12226 (2012).
3. F. Scotgnella, G.D. Valle, A.R.S. Kandada, M. Zavelani-Rossi, S. Longhi, G. Lanzani, and F. Tassone, Euro. Phys. J. B **86**, 154 (2013).
4. J.A. Faucheaux, A.L.D. Stanton, and P.K. Jain, J. Phys. Chem. Lett. **5**, 976 (2014).
5. A. Comin and L. Manna, Chem. Soc. Rev. **43**, 3957 (2014).
6. F. Hache, D. Ricard, and C. Flytzanis, J. Opt. Soc. Am. B **3**, 1647 (1986).
7. C. Flytzanis, F. Hache, M.C. Klein, D. Ricard, and P. Roussignol, in *Progress in Optics Vol. 29*, 1st ed., edited by E. Wolf (North Holland, Amsterdam, 1991) p. 340
8. T. Kuzuya, K. Itoh, and K. Sumiyama, J. Colloid Interface Sci. **319**, 565 (2008).
9. Y. Hamanaka, T. Hirose, K. Yamada, and T. Kuzuya, Opt. Mater. Exp. **6**, 275168 (2016).
10. P. Lukashev, W. R. Lambrecht, T. Kotani, and M. van Schilfgaarde, Phys. Rev. B **76**, 195202 (2007).
11. O. Madelung, *Semiconductors: Data Handbook*, 3rd ed. (Springer, Berlin, 2004), p. 455.
12. B. Palpant, in *Non-linear Optical Properties of Matter*, edited by M. G. Papadopoulos, A. J. Sadlej, and J. Leszczynski (Springer, Dordrecht, 2006) p.472.
13. P.B. Johnson and R.W. Christy, Phys. Rev. B **6**, 4370 (1972).
14. C. Kittel, *Introduction to Solid State Physics*, 7th ed. (John Wiley & Sons, New York, 1996) p. 150.